

Interannual variability of the spring Wyrtki Jet*

Kangping DENG¹, Xuhua CHENG^{1,2,3, **}, Tao FENG¹, Tian MA¹, Wei DUAN¹, Jiajia CHEN¹

¹ Hohai University, Nanjing 210098, China

² Southern Marine Science and Engineering Guangdong Laboratory (Zhuhai), Zhuhai 519000, China

³ Key Laboratory of Coastal Disaster and Defense (Hohai University), Ministry of Education, Nanjing 210098, China

Received Dec. 24, 2019; accepted in principle Feb. 4, 2020; accepted for publication May 28, 2020

© Chinese Society for Oceanology and Limnology, Science Press and Springer-Verlag GmbH Germany, part of Springer Nature 2021

Abstract Features of the interannual variability of the spring Wyrtki Jet in the tropical Indian Ocean are revealed using observation data and model output. The results show that the jet has significant interannual variation, which has a significant correlation with winter El Niño Modoki index ($R=0.62$). During spring after an El Niño (La Niña) Modoki event, the Wyrtki Jet has a positive (negative) anomaly, forced by a westerly (easterly) wind anomaly. The result of a linear-continuously stratified model shows that the first two baroclinic modes explain most of the interannual variability of the spring Wyrtki Jet (~70%) and the third to fifth modes together account for approximately 30%. Surface wind anomalies in the tropical Indian Ocean are related to the Walker circulation anomaly associated with El Niño/La Niña Modoki. The interannual variability of the spring Wyrtki Jet has an evident impact on sea surface salinity transport before the onset phase of the summer monsoon in the Indian Ocean.

Keyword: Equatorial Indian Ocean; Wyrtki Jet; interannual variability; El Niño/La Niña Modoki

1 INTRODUCTION

Between the summer and winter monsoon seasons, eastward surface jets flow along the equator with a high speed across almost the entire equatorial Indian Ocean (EIO). These high-speed eastward jets are called the Wyrtki Jets (Wyrtki, 1973). Since the seminal work of Wyrtki in 1973, many studies have focused on these strong eastward jets in the Indian Ocean (Molinari et al., 1990; Han et al., 1999, 2001, 2011; Han, 2005; Nagura and McPhaden, 2008, 2010a; Qiu et al., 2009; Gnanaseelan et al., 2012). The Wyrtki Jets develop as a direct response to the onset of westerlies in the EIO, which accounts for 81% of the Wyrtki Jet amplitude (O'Brien and Hurlburt, 1974). It has been widely accepted that the maximum strength of the jets lies at the surface and is located between approximately 75°E and 80°E. The speed of the Wyrtki Jets decreases with increasing depth, with the maximum speed exceeding 1 m/s at the surface (Wyrtki, 1973; Donguy and Meyers, 1995; Han et al., 1999).

There are strong seasonal and semiannual variations of the Wyrtki Jets in the EIO. The amplitude

of the semiannual signal is twice as large as the annual signal. A basin resonance in the Indian Ocean leads to a strong semiannual response that explains why the semiannual signal dominates the annual signal (Han et al., 1999). The Wyrtki Jets emerge initially in the central EIO (between 70°E and 75°E) after the onsets of equatorial westerlies and then propagate westward (Molinari et al., 1990; Han et al., 1999; Gnanaseelan et al., 2012; Deshpande and Gnanaseelan, 2013). The westward propagation of Wyrtki Jets is forced predominantly by the drifting westerlies and the Rossby waves pattern along the equator in the Indian Ocean (Han et al., 1999; Nagura and McPhaden, 2010b). Previous researchers used their models to reproduce the realistic spatial structure and strength of the Wyrtki Jets. The first and second baroclinic modes dominate the seasonal and semiannual variabilities of the surface currents in the tropical

* Supported by the National Key R&D Program of China (No. 2018YFA0605702), the National Natural Science Foundation of China (Nos. 41876002, 41776002), and the Fundamental Research Funds for the Central Universities (Nos. 2017B04714, 2017B04114)

** Corresponding author: xuhuacheng@hhu.edu.cn

Indian Ocean, which are influenced by both Rossby waves and wave resonance in addition to the direct wind forcing (Han et al., 1999; Nagura and McPhaden, 2010a; Chen et al., 2015). The reflected Rossby waves interfere with the semiannual signal propagation of the Wyrtki Jets in the eastern Indian Ocean, which weakens the semiannual signal of the jets near the eastern boundary. Under the impacts of Rossby waves and their reflection from the eastern boundary, the eastward Wyrtki Jets disappear within approximately 2 months after their genesis (Gnanaseelan et al., 2012). With a climatological velocity of the Wyrtki Jet at 70°E of 0.75 m/s in fall and 0.50 m/s in spring (Molinari et al., 1990), the former is stronger than the latter in climate with broader scale (Knox, 1976; Molinari et al., 1990). The precipitation during the summer and fall generates a thin mixed layer that considerably strengthens the fall Wyrtki Jet in the eastern Indian Ocean, and both spring and fall Wyrtki Jets reach approximately equal strengths under the influence of the Maldives (Han et al., 1999).

The equatorial currents in the tropical Indian Ocean also show significant intraseasonal variability (Han et al., 2001; Senan et al., 2003; Masumoto et al., 2005; Nagura and McPhaden, 2008; Chatterjee et al., 2013; Moum et al., 2014; Chen et al., 2019). As a significant intraseasonal event, Madden-Julian oscillation (MJO) accounts for most of the intraseasonal variation of winds in the tropical Indian Ocean during its active phase (November–May) (Lau and Wu, 2010; Lau and Waliser, 2012). Strong intraseasonal westerly anomalies exist in spring and fall in the EIO. Its strength is much higher during late spring, extending across almost the entire EIO, but weaker in fall (Prerna et al., 2019). Deshpande et al. (2017) showed that the intraseasonal variability of the spring Wyrtki Jet played an important role in the interannual variability of the jet. Strong tropical cyclones over the Bay of Bengal also influence the strength of the fall Wyrtki Jet (Sreenivas et al., 2012). In addition, the significant intraseasonal westerly anomaly in the EIO in spring associated with the strong MJOs is the most likely dominant factor for anomalous strong spring Wyrtki Jet behavior (Duan et al., 2016).

Previous researchers have paid more attention to the fall Wyrtki Jet, and the variability of the fall Wyrtki Jet shows a distinct pattern. Over longer time scales, Wyrtki Jets exhibit strong interannual variability, which is caused by the interannual variability of the westerly wind forcing along the equator. Many previous works have demonstrated

that the interannual variability of the fall Wyrtki Jet is associated with the Indian Ocean Dipole (IOD) and El Niño/La Niña events (Nyadjro and McPhaden, 2014; Zhang et al., 2014; Zhang et al., 2016). When a positive IOD event occurs, an easterly wind anomaly associated with the sea surface temperature (SST) anomaly appears and weakens the fall Wyrtki Jet, and vice versa (Rao et al., 2002; Thompson et al., 2006; Subrahmanyam et al., 2011; Gnanaseelan et al., 2012). Due to the smaller amplitude of the spring Wyrtki Jet than the fall one, the spring Wyrtki Jet has been less studied. Joseph et al. (2012) proposed that the spring Wyrtki Jets significantly weakened during 2006 to 2011 and even reversed during 2008, and the mechanism for their weakening is not yet clear. They also suggested that the correlation between spring Wyrtki Jet and El Niño was not significant.

To explore the interannual variability of the spring Wyrtki Jet, the potential impacts of interannual climate modes, the IOD and El Niño-Southern Oscillation (ENSO), should be taken into consideration. A number of studies have suggested that the IOD has significant impacts on the fall Wyrtki Jet (Rao et al., 2002; Thompson et al., 2006; Subrahmanyam et al., 2011; Gnanaseelan et al., 2012; Nyadjro and McPhaden, 2014; Zhang et al., 2014; Zhang et al., 2016). The IOD reaches its peak during September–November and has dissipated in winter, so it is unlikely to affect the Wyrtki Jet in the following spring. In contrast, the ENSO can affect the atmosphere-ocean systems in the Indian Ocean during the post-ENSO spring and summer through the effect of the Indo-western Pacific Ocean capacitor (Xie et al., 2009, 2010, 2016). At the peak phase of El Niño events, positive SST anomalies usually appear in the tropical Indian Ocean and reach their peak after three months (Klein et al., 1999). The atmospheric circulation acts as a ‘bridge’ to link SST anomalies in the central equatorial Pacific with those in the Indian Ocean (Lau, 1997; Alexander et al., 2002; Larkin and Harrison, 2005; Xie et al., 2002, 2009). The warming of the tropical Indian Ocean acts as a capacitor that causes an increased tropospheric temperature anomaly by a moist-adiabatic adjustment (Xie et al., 2009). The capacitor effect has a significant impact on the surface wind in the tropical Indian Ocean in spring and summer following El Niño events, which may have a potential impact on the spring Wyrtki Jet.

In addition to the canonical ENSO events, there also exists an abnormal warming event in the central Pacific Ocean, known as the El Niño Modoki event

(Ashok et al., 2007). The evolutions and influence of Niño Modoki events differ from those of canonical ENSO events. Importantly, the thermodynamic mechanisms and associated atmospheric responses are distinctly different between the Niño Modoki and the canonical ENSO events (Yu and Kao, 2007; Wang, 2017; Dandi et al., 2020). Due to the different locations of SST anomalies, the Niño Modoki events cause different atmosphere circulation anomalies in the tropical Indian Ocean (Ashok and Yamagata, 2009), which also has potential impacts on the interannual variability of the spring Wyrtki Jet.

The eastward spring Wyrtki Jet modulates the transport of water mass, heat, and salinity along the equator and then alters the upper-layer stratification in the eastern EIO before the onset of the summer monsoon (Reppin et al., 1999; Deshpande and Gnanaseelan, 2013; Deshpande et al., 2017; Wang, 2017), which has a potential impact on the onset of the summer monsoon. Although the spring Wyrtki Jet is weaker than the fall one, greater transport of the spring Wyrtki Jet than the fall one near 80°E was proposed by Donguy and Meyers (1995). The interannual variability of the spring Wyrtki Jet has been less studied. Considering the importance of the tropical Indian Ocean circulation and the significant impacts of the spring Wyrtki Jet on the zonal heat and salt transport before the onset of the summer monsoon, we focus on the interannual variability of the spring Wyrtki Jet in this study.

2 DATA AND METHOD

The surface current velocity data from the Ocean Surface Current Analysis Realtime (OSCAR) database used in this study has a horizontal resolution of 1/3°×1/3° and a time span from January 1993 to December 2016 with a 5-day mean resolution. The current data of Research Moored Array for African-Asian-Australian Monsoon Analysis and Prediction (RAMA) acoustic doppler current profile (ADCP) mooring along the equator located at 80.5°E and 90°E from January 2005 to December 2014 are used in this study. They are available in 5 m (10 m) vertical resolution at 80°E (90°E). The monthly and 5-day mean velocities and salinity are derived from the Oceanic General Circulation Model for the Earth Simulator (OFES) (Sasaki et al., 2004; Masumoto et al., 2008). With a correlation of 0.92 with the RAMA data and 0.88 with the OSCAR data, the current data from OFES, which has a much longer time series, can be used to study the low-frequency variations of

Wyrtki Jets. The monthly mean Outgoing Longwave Radiation (OLR) and Niño 3.4 index from the National Oceanic and Atmospheric Administration (NOAA) are also used. To calculate the El Niño Modoki index (EMI), we obtained the monthly gridded 1°×1° sea surface temperature (SST) data for January 1990 to December 2018 from NOAA OISST. The equation for calculation is:

$$\text{EMI} = [\text{SSTA}]_A - 0.5 \times [\text{SSTA}]_B - 0.5 \times [\text{SSTA}]_C. \quad (1)$$

Ashok et al. (2007) came up with this equation, and the outer subscripts of the parentheses in Eq.1 represent three regions: A (165°E–140°W, 10°S–10°N), B (110°W–70°W, 15°S–5°N), and C (125°E–145°E, 10°S–20°N).

In addition, to explore the mechanism of interannual variation of the spring Wyrtki Jet, a linear-continuously stratified (LCS) model is used in the study. The LCS model has been applied in many studies on circulations and sea level in the Indian Ocean (McCreary et al., 1996; Miyama et al., 2003, 2006; Suresh et al., 2013; Cheng et al., 2017). In this study, we used a modified version discussed by Miyama et al. (2006). The LCS equations are simplified equations of linearized motion based on a background state of rest with the Brunt-Väisälä frequency $N_b(z)$. $N_b(z)$, which is depth dependent, is derived from the World Ocean Database (WOD) 2001 and averaged within the region 1°S–1°N and 40°E–100°E. In the model, the ocean bottom is flat with depth $D=4500$ m. Vertical eddy viscosity and diffusivity coefficients are calculated as $\nu(z)=A/N_b^2(z)$, where $A=8.84\times10^{-4}$ cm²/s³. The solutions of the model can be written as the expansions of the vertical modes of the system:

$$q(x, y, z, t) = \sum_{n=1}^N q_n(x, y, t) \psi_n(z), \quad (2)$$

q is one of u , v , and p , and $\psi_n(z)$ is the normalized vertical structure function of the n -th mode. At the surface, $\psi_n(0)=1$. The expansion coefficients satisfy

$$u_{nt} + fk \times u_n = -\frac{1}{\rho_0} \nabla p_n - \frac{A}{c_n^2} u_n + A_h \nabla^2 u_n + \frac{Z_n}{H_n} \tau, \quad (3a)$$

$$\frac{1}{c_n^2} p_{nt} + \nabla u_n = -\frac{A}{c_n^2} p_n, \quad (3b)$$

where c_n is the Kelvin-wave speed of the n -th mode. The n -th mode, which is forced by the surface wind stress, is determined by $Z_n = \int_{-D}^0 Z(z) \psi_n(z) dz$ and $H_n = \int_{-D}^0 \psi_n^2(z) dz$. With these hypotheses and definitions, the solutions of the equation can be written as a linear

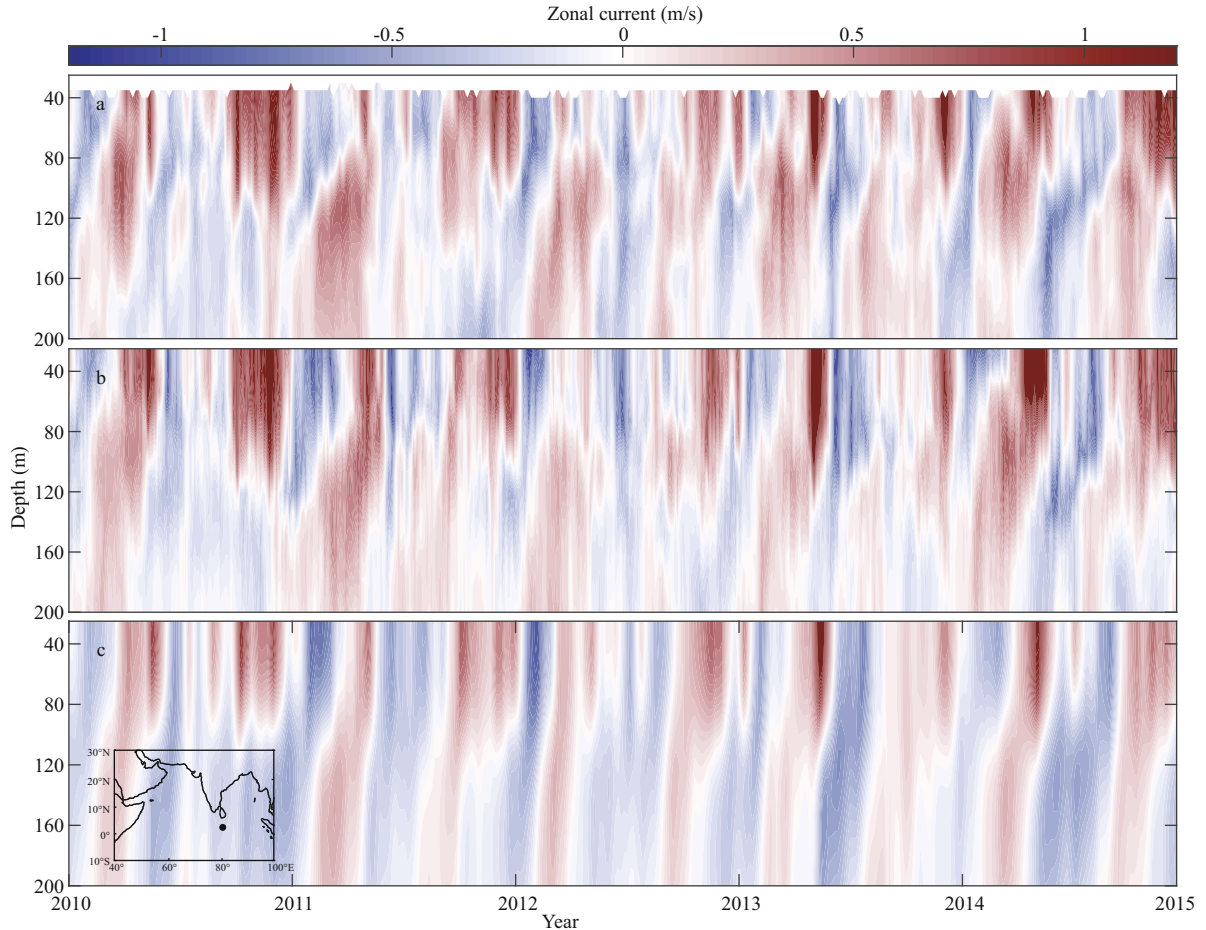


Fig.1 Time-depth section of zonal current (m/s) at 80°E , 0° (black dot) from the RAMA (a), OFES (b), and LCS (c) model in the upper 200 m

superposition of different baroclinic and barotropic vertical modes of the system. This simple linear model was set up for the region of the Indian Ocean between 30°E and 120°E , 30°S and 25°N . The LCS model is forced by the wind stress derived from National Centers for Environmental Prediction (NCEP) surface wind (NCEP run) and ERA-Interim (ERA-I) surface wind data from the European Centre for Medium-Range Weather Forecasts (ECMWF run) for the period 1979–2015 (Dee et al., 2011). The daily NCEP surface wind data with a horizontal resolution of $1.875^{\circ} \times 1.875^{\circ}$ and OMEGA data at different pressure level and ECMWF surface wind data with a horizontal resolution of $0.75^{\circ} \times 0.75^{\circ}$ are used in this study.

3 OBSERVATION AND MODEL VALIDATION

Figure 1a shows the zonal current up to a depth of 200 m from RAMA observations at 80°E and 0°N from 2010 to 2014. The eastward Wyrtki Jets during April to May and June to September in the upper 100 m ocean can be clearly seen. The eastward

equatorial undercurrent during January to March at the subsurface (at 60 to 120 m) is also distinct. The spring Wyrtki Jet shows significant interannual variability. During 2011 and 2012, the spring Wyrtki Jet was quite weak. In contrast, the spring Wyrtki Jet in 2013 was stronger than normal. Its speed exceeded 1 m/s, and the affected depth reached 110 m. Both the OFES and LCS model reproduce the variability of zonal currents in the EIO quite well (Fig.1b & c), except that the amplitude of the zonal current is stronger (weaker) in the OFES (LCS model).

The spring Wyrtki Jet is observed during the winter and summer monsoon transition periods. It was initially observed near 75°E in the western equatorial ocean starting in mid-April, then gradually strengthened and presented mainly in May (McPhaden et al., 2015). Therefore, we focus on the variations of Wyrtki Jet in May in this study. Figure 2 shows the climatological horizontal currents in May from the OSCAR, OFES and LCS model averaged in the upper 30 m over the period of 1993–2014. The May Wyrtki Jet exists in the equatorial regions (5°S – 5°N), and its

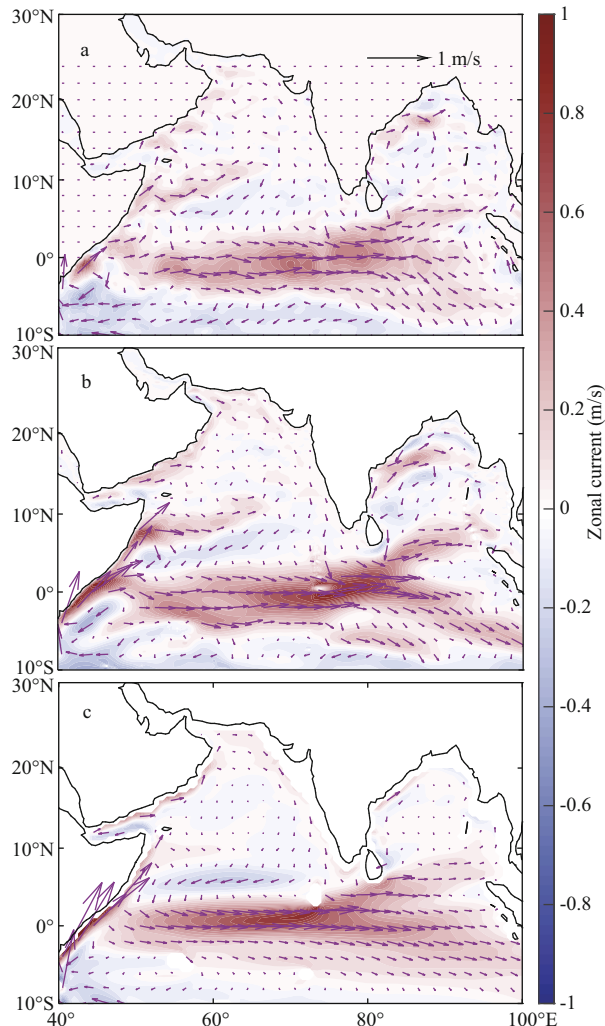


Fig.2 Map of climatology zonal current speed (shading, m/s) and current vectors (m/s) in May from the OSCAR (a), OFES (b), and LCS (c) model

The currents from the OFES and LCS model are calculated in the upper 30 m.

axis bends to the south of the equator. Observations and models all show that the maximum strength of the spring Wyrtki Jet exceeds 0.7 m/s in the eastern part (approximately 75°E–80°E) in May. The LCS model and OFES output capture the horizontal distribution of the strong eastward current well during spring. The correlation coefficient between the LCS model and OSCAR/OFES currents exceeds 0.8 in the Wyrtki Jet region and exceeds 0.7 in other regions as well. Compared to the results from the OFES and the OSCAR data, the Wyrtki Jet from the LCS model is weaker in the upper 30 m. At the end of the current, a bifurcation occurred there. The southern branch is stronger than the northern branch. The OFES and LCS model are consistent with the OSCAR data in the horizontal structure and with the RAMA data in

the vertical structure. With a much longer time span, OFES data have been considered reliable in describing the interannual variations of the Wyrtki Jet in spring. The LCS model can essentially simulate the characteristics of Wyrtki Jets, which is an applicable model to verify the interannual variability mechanism of the spring Wyrtki Jet.

4 INTERANNUAL VARIATION

The horizontal currents in May from 1993 to 2016 from the OSCAR data are shown in Fig.3. The spring Wyrtki Jet in 1994, 1999, 2000, 2008, and 2011 was weaker, while it was stronger in 2002, 2004, 2013, and 2016. What causes such remarkable interannual variations of the zonal current along EIO in May? A number of studies have suggested that the ENSO can influence the atmosphere-ocean systems in the Indian Ocean during the following spring and summer due to the Indo-western Pacific Ocean capacitor (Xie et al., 2009, 2010, 2016; Chowdary et al., 2017; Srinivas et al., 2019). However, the correlation between the average of December, January, and February (DJF) Niño3.4 index and the OSCAR zonal current at 80°E, 0°/90°E, 0° in May is not significant ($R=-0.26/-0.21$). For the OFES zonal current, the correlation coefficient is $-0.20/-0.29$. The weak lag correlation between the ENSO and spring Wyrtki Jet indicates that the impact of conventional ENSO events on the spring Wyrtki Jet is not significant.

Since the 1970s, events of SST anomalies in the central Pacific have increased, which is not similar to conventional El Niño events. The new type El Niño is called El Niño Modoki or central Pacific (CP) El Niño (Ashok et al., 2007; Ashok and Yamagata, 2009; Yeh et al., 2009). The impacts of El Niño Modoki on the atmosphere-ocean system are quite different from those of conventional El Niño (Ashok et al., 2007; Ashok and Yamagata, 2009; Yeh et al., 2009). It is possible that El Niño Modoki events have impacts on the surface wind in the tropical Indian Ocean through teleconnections and then alter the equatorial ocean current. Fig.4a shows the time series of the EMI over 1993–2016 derived from monthly mean OISST data using equation (1). The zonal currents in May at 80°E, 0°/90°E, 0° from OSCAR have a positive correlation with the monthly mean EMI in January (0.54/0.47, significant at the 95% confidence level). The correlation between the zonal current in May averaged in the upper 30 m at 80°E, 0°/90°E, 0° from OFES and the EMI in January is 0.60/0.62 (Fig.4b&c). The significant lag correlation between the EMI and zonal

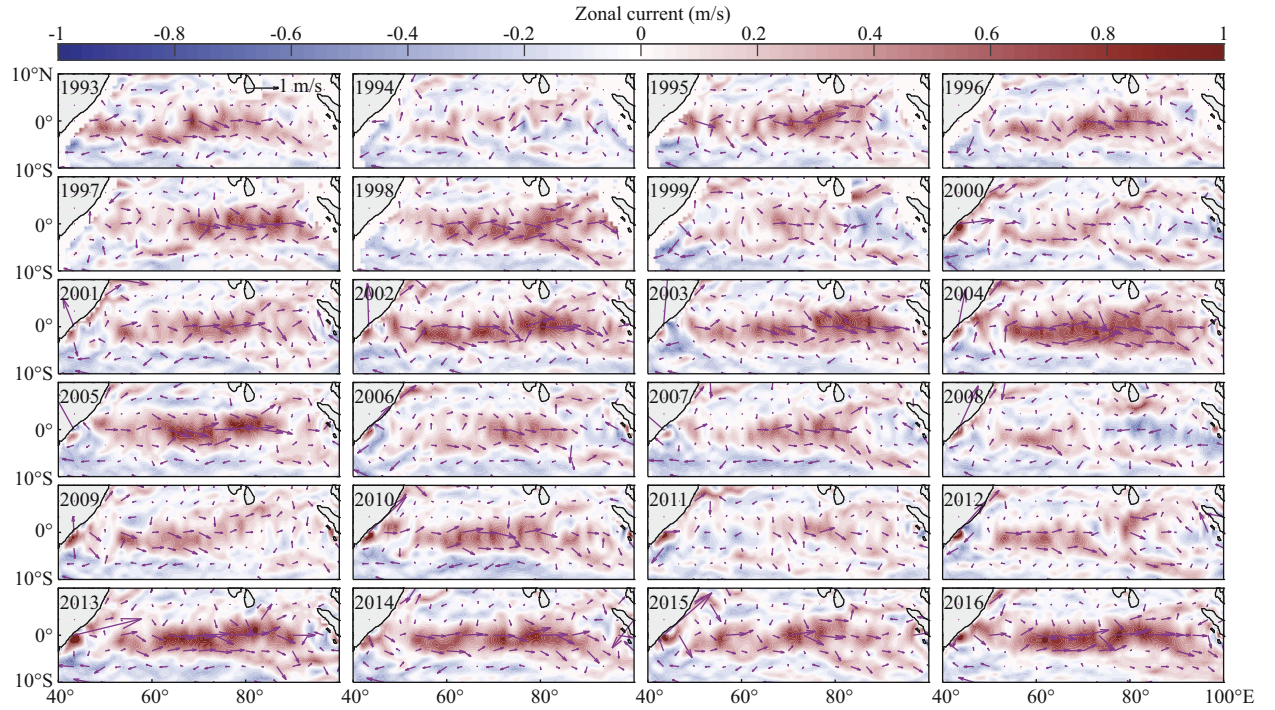


Fig.3 OSCAR zonal current speed (shading, m/s) and current vectors in May from 1993 to 2016

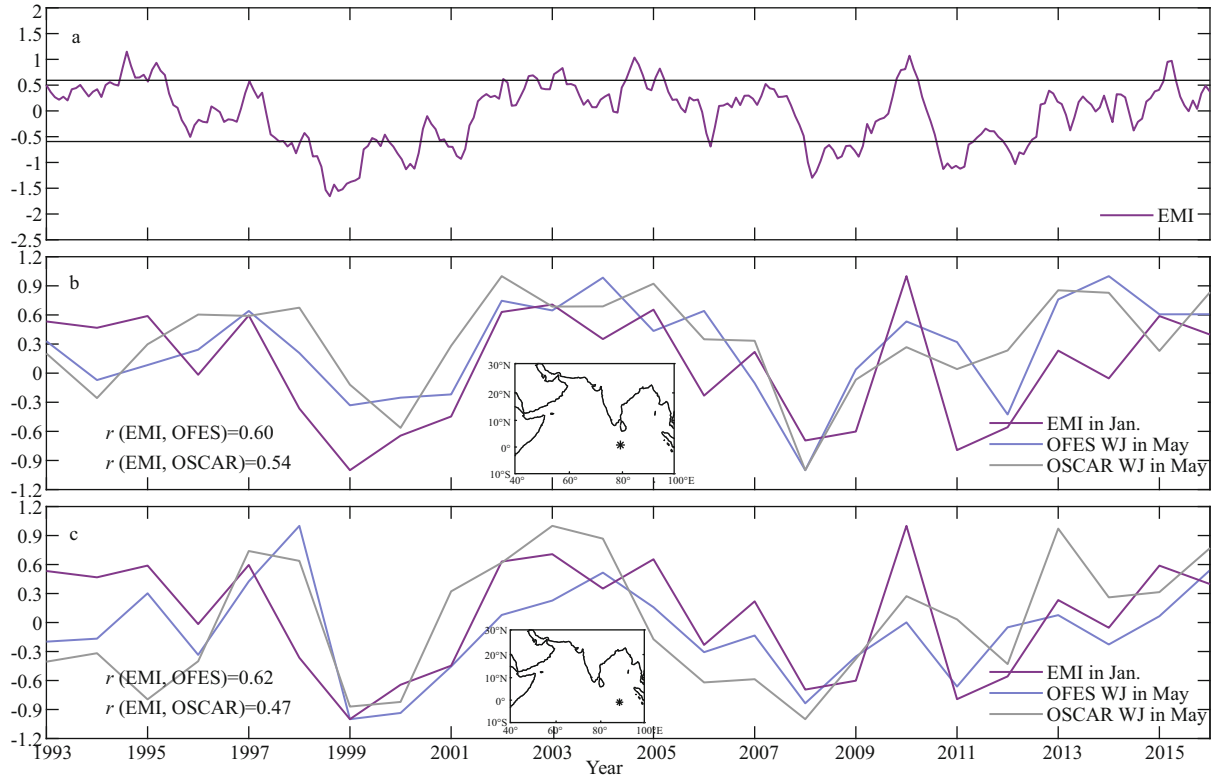


Fig.4 Normalized time series of the EMI calculated by monthly OISST data from 1993 to 2016 (a); time series of the EMI in January and normalized zonal currents from OFES and from OSCAR in May at 80°E, 0° (b) and 90°E, 0° (c)

The black lines in (a) indicate the one standard deviation of the EMI. These datasets are standardized.

current in the EIO indicates that the interannual variations of the spring Wyrtki Jet are likely associated with El Niño Modoki events. Besides interannual

variability, the spring Wyrtki Jet also had significant decadal variability. Its strength had a decrease trend over 2003–2007 and increase trend over 2008–2015.

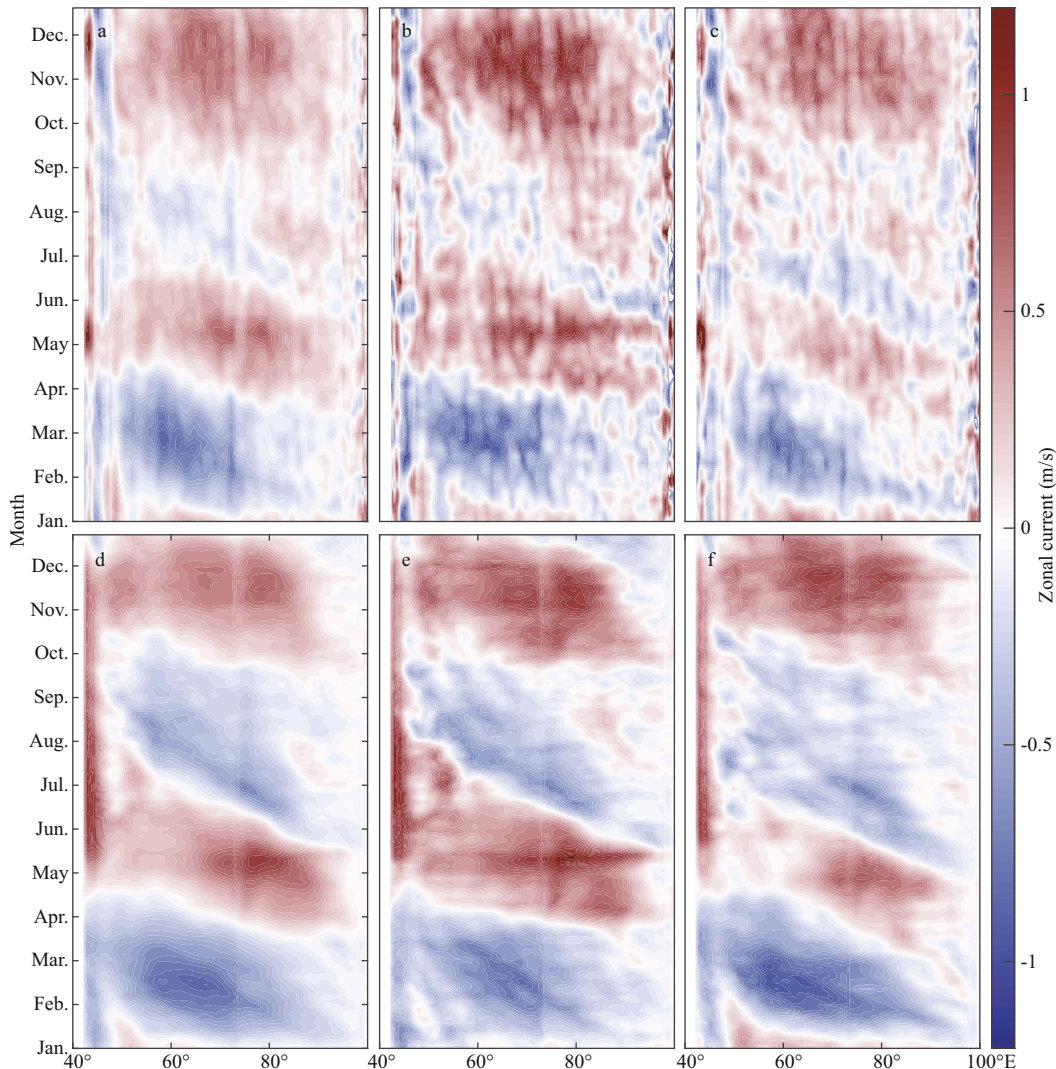


Fig.5 Longitude-time diagrams of the annual cycle of zonal currents (averaged between 1°S and 1°N) from OSCAR (a–c); composite in years after El Niño Modoki events (b); composite in years after La Niña years (c); the same as (a–c) except from OFES with upper 30-m mean (d–f)

To show the relationship of the spring Wyrtki Jet to Niño Modoki in detail, a composite method was used. We took the years when the EMI in winter was greater than one standard deviation (STD, 1994, 2002, 2004, and 2009) to be the El Niño Modoki years and less than one negative STD (1998, 1999, 2007, 2008, 2010, and 2011) to be the La Niña Modoki years, which is consisted with work of previous studies (Shinoda et al., 2011; Yuan and Yan, 2013; Wang et al., 2018). We took the spring in the following years (1999, 2000, 2008, 2009, 2011, and 2012) to perform a composite analysis. The composite annual cycle of zonal currents averaged between 1°S and 1°N from OSCAR and OFES are shown in Fig.5. The climatology spring Wyrtki Jet starts in early April, reaching its peak in May, and dissipates in early June (Fig.5a & d). The multi-year composite of the Wyrtki

Jet in May following the El Niño Modoki and La Niña Modoki events from OSCAR and OFES shows strong interannual variations. Compared with the climatology mean, the strength of the spring Wyrtki Jet following the El Niño Modoki events was enhanced. In the spring following the La Niña Modoki events, the Wyrtki Jet is weakened significantly and almost disappears in mid-May (Fig.5).

Figure 6 shows the composite upper-layer current in May. Following the El Niño Modoki events, there is a stronger Wyrtki Jet in May, which extends from 50°E to 90°E . Compared with the climatology mean in Fig.2, the Wyrtki Jet has a positive anomaly of approximately 0.3 m/s in May after the El Niño Modoki events. The May Wyrtki Jet has negative anomaly exceeding 0.45 m/s from OSCAR data following the La Niña Modoki events, with a

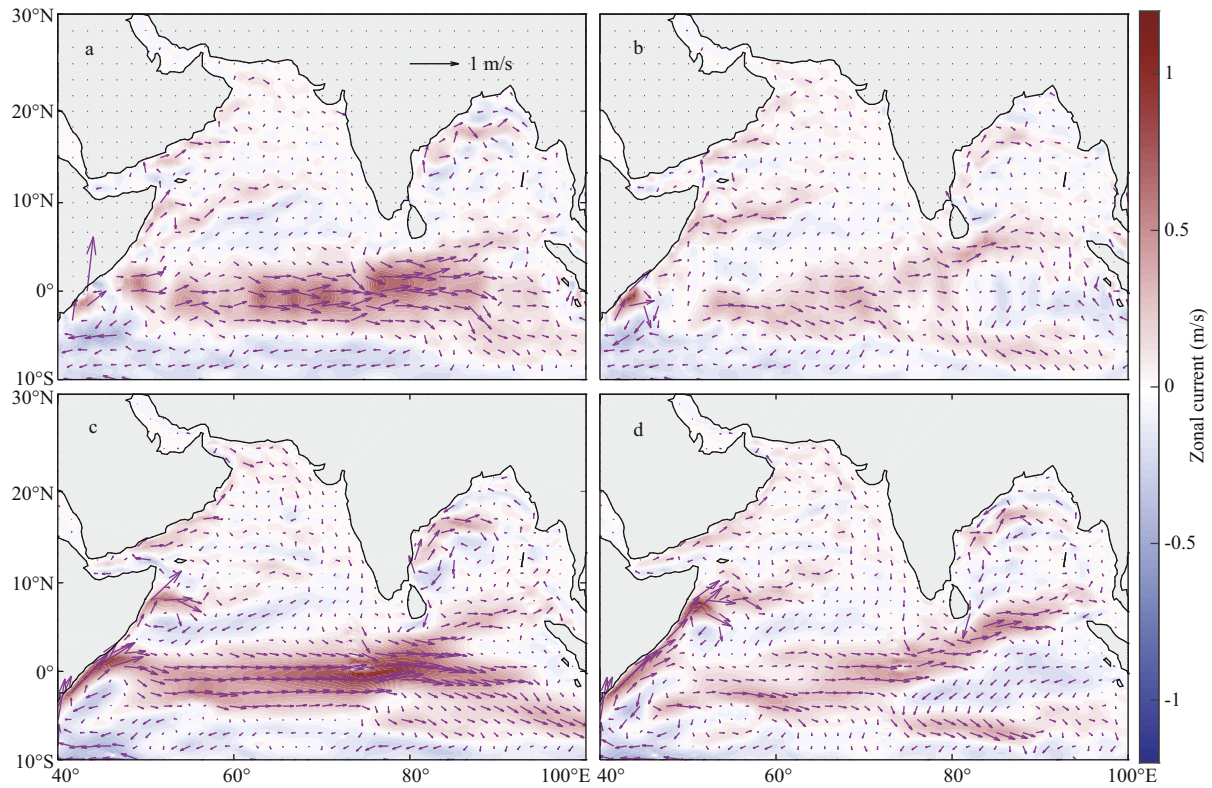


Fig.6 Composite zonal current (shading, m/s) and current vectors in May from OSCAR in years after El Niño Modoki events (a) and La Niña Modoki events (b); the same as (a, b) except from OFES with upper 30-m mean (c, d)

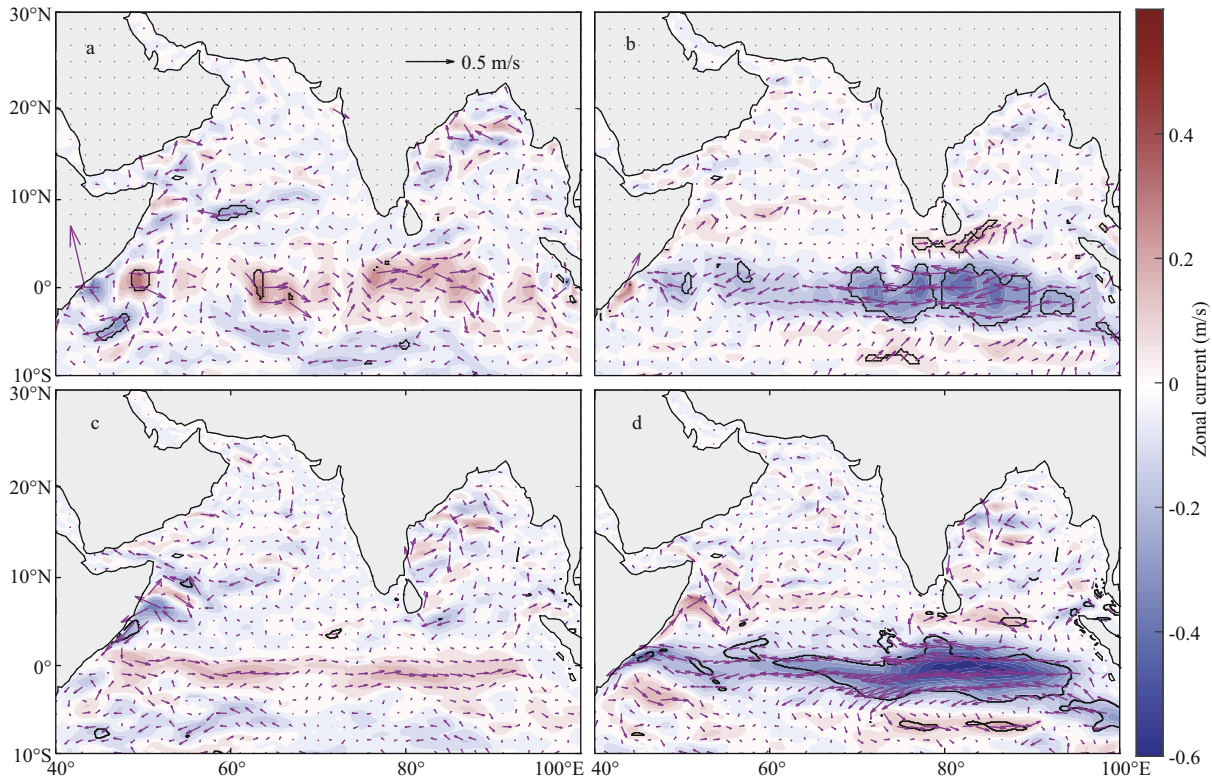


Fig.7 Composite zonal current speed anomalies (shading, m/s) and current vectors anomalies in May from OSCAR in years after El Niño Modoki events (a) and La Niña Modoki events (b); the same as (a, b) except from OFES with upper 30-m mean (c, d)

The black contour denotes values statistically significant at the 95% level.

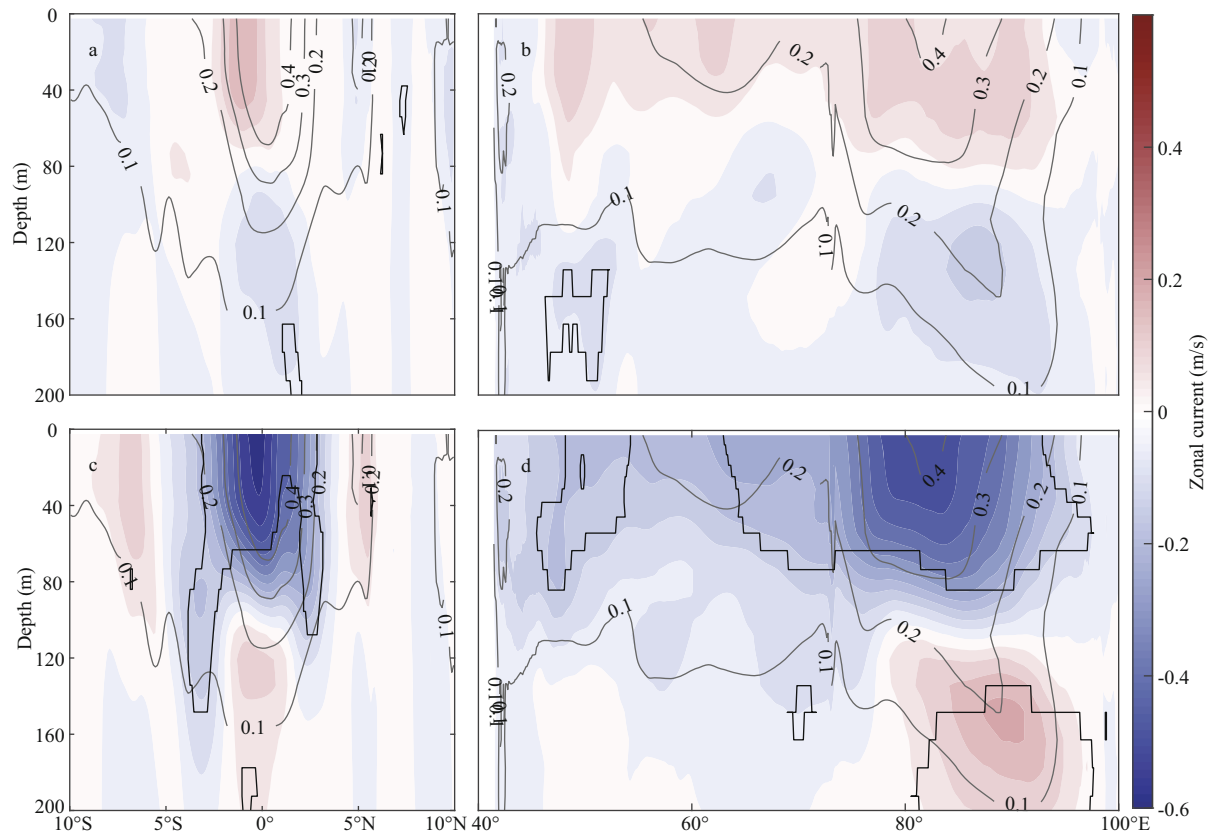


Fig.8 Latitude-depth diagram of composite zonal current anomalies (shading, m/s) in May in years after El Niño Modoki events at 80°E (averaged between 79°E and 81°E) (a); longitude-depth diagram of composite zonal current anomalies (shading, m/s) in May after El Niño Modoki events at 0° (averaged between 1°S and 1°N) (b); the same as (a, b) except after La Niña Modoki events (c, d)

The currents are from OFES. The gray lines indicate the standard deviation (STD) of the zonal current in May and the black contour denotes values statistically significant at the 95% level.

significance level above 95% in most of the Wyrtki Jet region (Figs.6 & 7). Both positive (0.32 m/s) and negative (0.48 m/s) anomalies of the May Wyrtki Jet mainly exist in the eastern EIO. The correlation coefficient between the OSCAR zonal velocity anomaly and EMI exceeds 0.5 in most of the Wyrtki Jet region (significant at the 95% confidence level). Similar analyses from OFES with a weaker positive anomaly (0.21 m/s) and a stronger negative anomaly (0.59 m/s) are also shown in Fig.7c & d.

The vertical distribution of the composited zonal velocity and its interannual STD along the 80°E section and the equator between 40°E and 100°E are shown in Fig.8. A strong interannual STD of zonal velocity is found in the eastern EIO mainly. Generally, the maximum interannual STD is located near the maximum of the zonal velocity. The composited zonal velocity anomaly in May following an El Niño Modoki event exists mainly in the upper 80 m, which is relatively uniform along the equator but slightly higher between 80°E and 90°E. Strong negative

velocity anomalies exist mainly east of the Maldives following La Niña Modoki events. The strong negative anomalies reach a depth of 110 m, and their maximum value is up to 0.5 m/s. The composite analysis shows that the zonal current anomaly in the EIO associated with Niño Modoki events does not simply show an inverse phase. Its strength and spatial distribution are obviously asymmetrical during El Niño and La Niña Modoki events. The relationship of the spring Wyrtki Jet to La Niña Modoki events is stronger than that to El Niño Modoki events. The La Niña Modoki forcing has a significant impact on the spring equatorial zonal current between 50°E and 90°E. These significant anomalous behaviors can be clearly observed in the OSCAR and OFES data. How do the Niño Modoki events affect the spring Wyrtki Jet? What is the mechanism of these anomalies? We will conduct further analysis in the next section.

5 MECHANISM

Since the spring Wyrtki Jet is significantly related

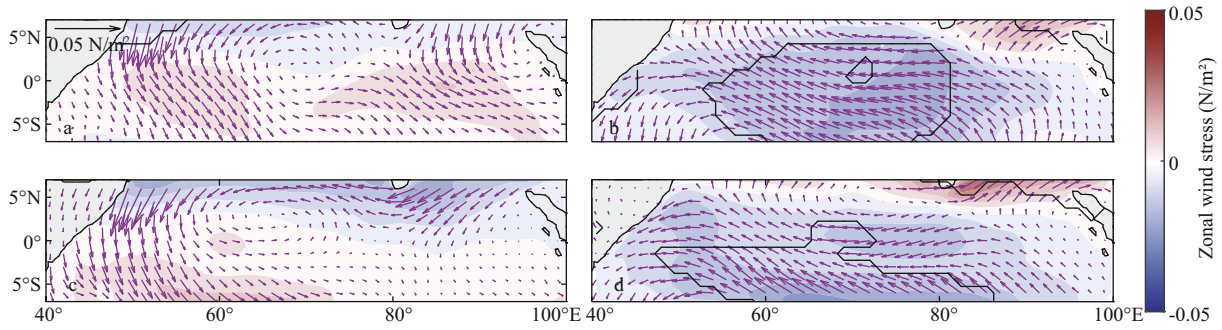


Fig.9 Composite zonal wind stress anomalies (shading, N/m^2) and wind stress vector anomalies (N/m^2) from NCEP after El Niño Modoki events (a) and La Niña Modoki events (b); the same as (a, b) except from ECMWF and the black contour denotes values statistically significant at the 90% level (c, d)

to Niño Modoki events, it is necessary to know the mechanisms connecting them. Previous studies have shown that the wind stress in the tropical Indian Ocean is the dominant force on variations of Wyrtki Jets at different time scales (Wyrtki, 1973; Nagura and McPhaden, 2010b; Gnanaseelan et al., 2012). Based on previous studies, we speculate that the wind stress anomaly associated with Niño Modoki events is likely the dominant factor driving the Wyrtki Jet anomaly in spring. To confirm our assumption, we performed a composite analysis of the wind stress.

As shown in Fig.9, the zonal wind stress anomalies in May dominate the EIO, with a significance level above 90% in most of the EIO region. During the peak spring Wyrtki Jet periods, the westerlies in May after El Niño Modoki events are slightly stronger than the climatological wind. The westerly wind anomalies after El Niño Modoki events and visible easterly wind anomalies after La Niña Modoki events exist mainly in EIO. The latter is more than twice as strong as the former. Compared with the results of the NCEP data, the wind anomalies from ECMWF are slightly weaker.

Composite longitude-time wind stress anomalies with regional averages (1°S – 1°N) along the equator from NCEP are shown in Fig.10a & b. A westerly wind anomaly was observed starting in early April in the western EIO (50°E – 70°E) and then extending eastward after El Niño Modoki events, which persisted for more than two months. This relatively weak westerly wind anomaly drives a weak eastward zonal current anomaly in the EIO (Fig.7a & c). Following a La Niña Modoki event, a wider range of easterly anomalies ($0.025 \text{ N}/\text{m}^2$) dominates the entire EIO from April to June. This significant easterly anomaly emerges initially in the western Indian Ocean and gradually propagates to the east until it overlies the entire EIO. The results from the ECMWF

are similar to those of the NCEP, but with a slightly weaker strength (Fig.10c & d).

The fundamental dynamics of the Wyrtki Jets are linear (Han et al., 1999, 2001, 2011; Nagura and McPhaden, 2010a). The aforementioned studies show that wind stress anomalies are the dominant factors for interannual variations of the spring Wyrtki Jet. In this study, using the LCS model forced only by surface wind (NCEP run/ECMWF run) allows us to verify the effect of wind forcing on the interannual variability of the spring Wyrtki Jet.

As shown in Fig.11, zonal current anomalies exist in the tropical Indian Ocean in May from the LCS model forced by NCEP wind (Fig.11a & b). A weak positive westerly wind anomaly in May after El Niño Modoki events leads to a much weaker response of the surface current. The maximum positive anomaly of the zonal current is less than 0.1 m/s . After La Niña Modoki events, the surface zonal current velocity along the equator sharply reduced with a maximum negative anomaly of 0.4 m/s . Compared with the results based on the OSCAR and OFES current data (Fig.7), the pattern of current anomalies for the period 1993–2014 based on the LCS model were virtually identical but with weaker in the respective composite years. The ECMWF run also shows similar results to the NCEP run (Fig.11c & d). During May after the La Niña Modoki events, a patch of easterly wind anomaly exists between 50°E – 90°E along the equator (Fig.9b & d), which drives Ekman transport poleward and induces upwelling along the equator. The upwelling signals propagate eastward as Kelvin waves. Corresponding to negative sea surface height anomalies, westerly zonal current anomalies are generated according to geostrophic balance (Fig.11b & d).

The first two baroclinic modes explain approximately 70% of the spring Wyrtki Jet anomaly,

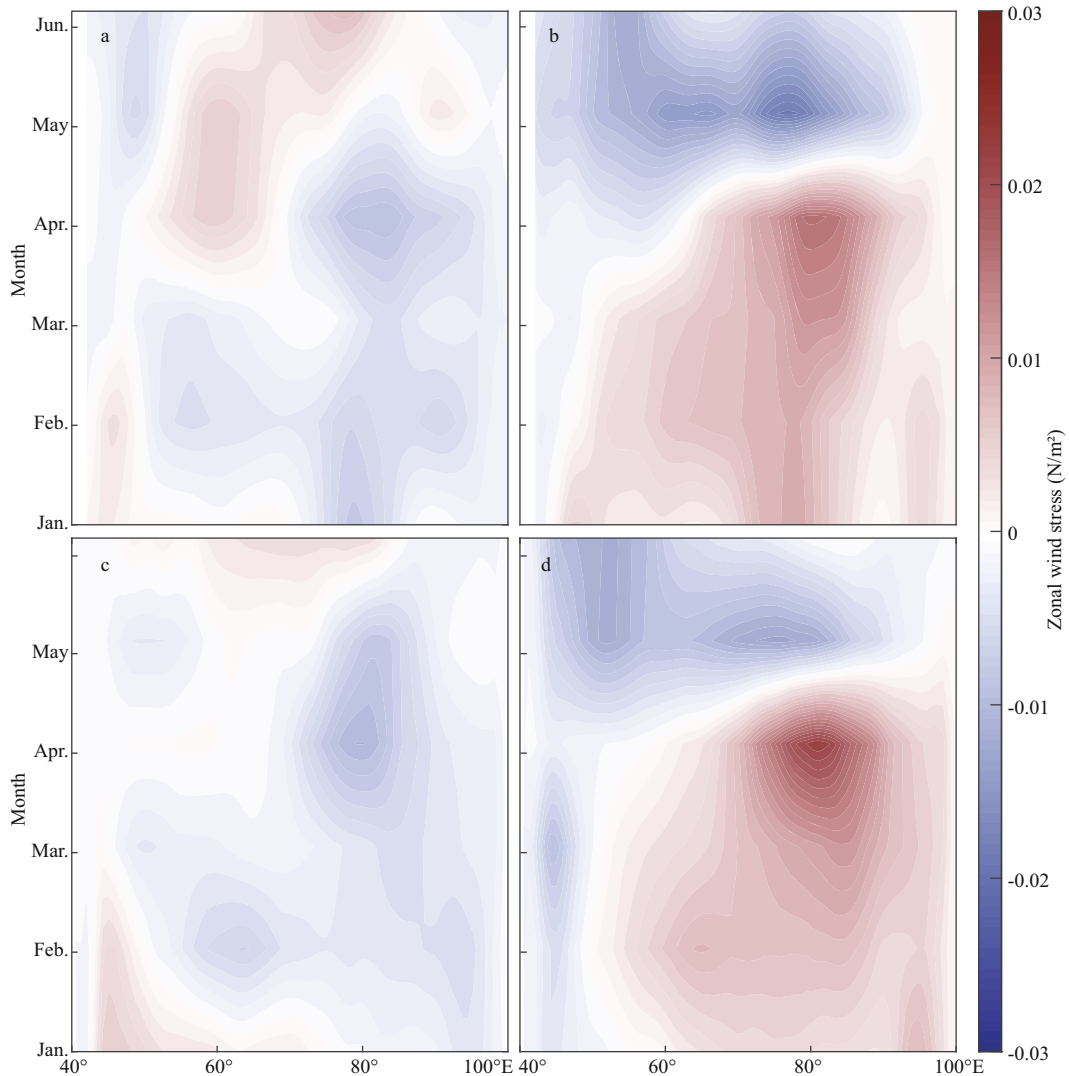


Fig.10 Longitude-time diagrams of zonal wind stress anomalies (averaged between 1°S and 1°N , N/m^2) from NCEP (a, b), composite in the years after El Niño Modoki events (a), composite in the years after La Niña events (b) and same as (a, b) except from ECMWF (c, d)

and the second mode plays a dominant role (Fig.12), which is consistent with the results of Chen et al. (2015). The third to fifth modes together account for approximately 30% of the spring Wyrtki Jet anomaly, and this part of the anomaly is confined to a narrow region along the equator. The zonal current anomalies forced by the two kinds of wind have similar structures with the OSCAR and OFES results. The vertical structure from the LCS model in the years after Niño Modoki events also incorporates the OFES results but with a deeper affected depth (Fig.13). The results from the LCS model indicate that anomalous wind is the dominant factor for the anomalous spring Wyrtki Jet. By conducting LCS model experiments, it is determined that the anomalous equatorial westerly associated with the Niño Modoki events play a

dominant role in the interannual variation of the spring Wyrtki Jet.

The Walker circulation anomaly induced by Niño Modoki may be the main cause of surface wind anomalies in the tropical Indian Ocean. Figure 14 shows the SST, OLR, and wind anomalies during mature and decaying phase of La Niña Modoki events over the Pacific and Indian Ocean. Negative SST anomalies are located in the central equatorial Pacific and EIO, while positive anomalies appear in the eastern of Maritime Continent region during the peak of La Niña Modoki events (Fig.14a–c). The SST anomalies during El Niño Modoki events are opposite, but with a weaker amplitude (not shown in this paper). In the decaying period of the La Niña Modoki events, remarkable negative SST anomalies appears in the

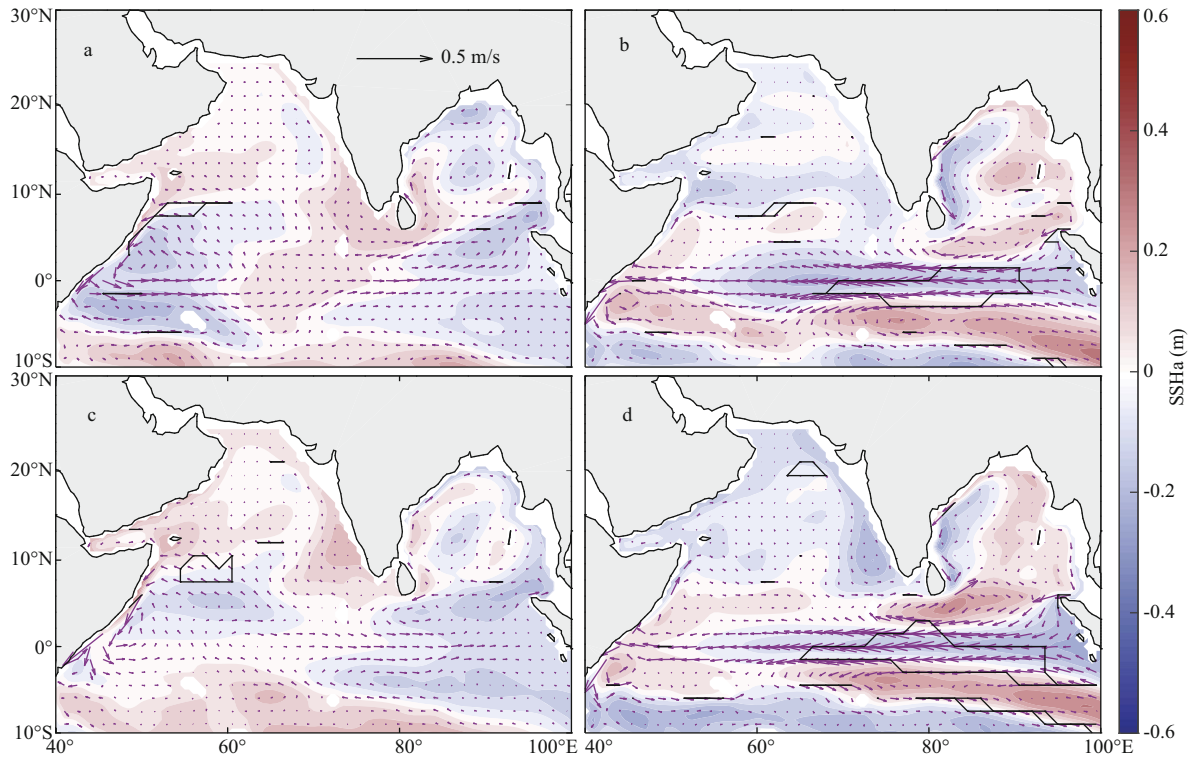


Fig.11 Composite current anomalies (vector, averaged in the upper 30 m, m/s) and SSH anomalies (shading, m) in May from the LCS model forced by NCEP wind stress in years after El Niño Modoki events (a) and La Niña Modoki events (b) onto the first 5 modes; the same as (a, b) except from the LCS model forced by ECMWF wind stress (c, d). The values surrounded by the black contours are statistically significant at the 95% level.

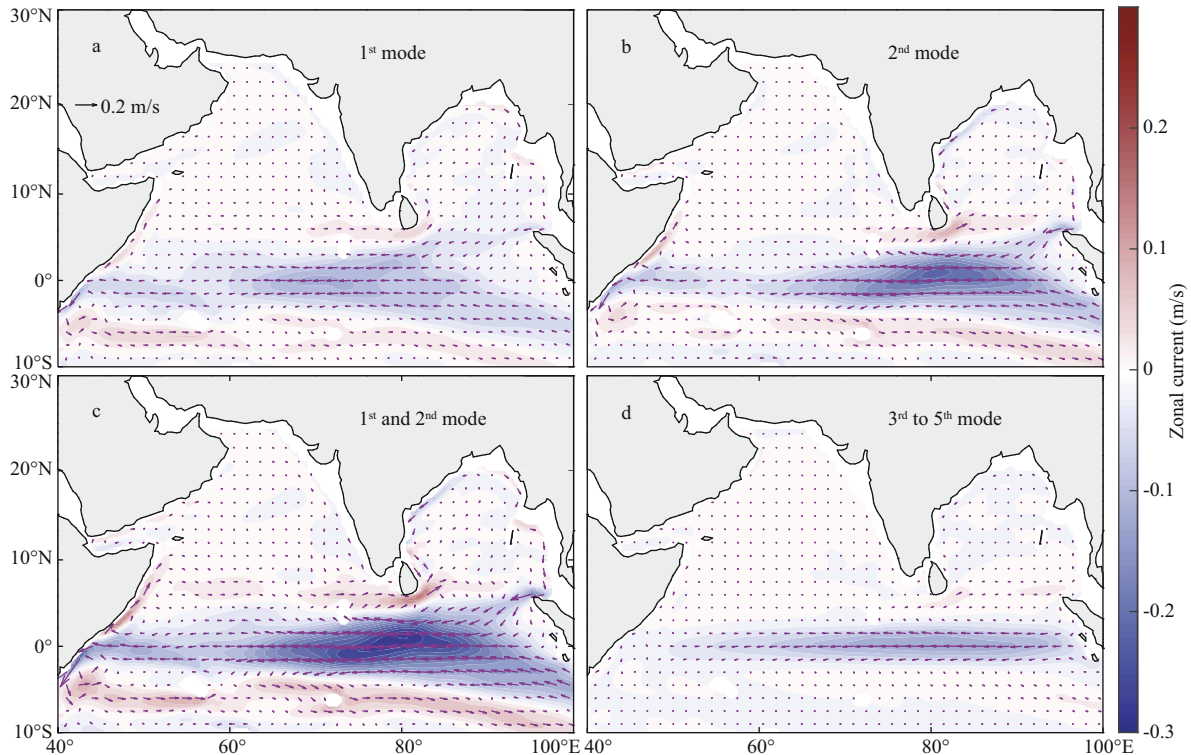


Fig.12 Composite zonal current speed anomalies (shading, m/s) and current vector anomalies (m/s) in May from the LCS model forced by ECMWF wind in the first mode (a), second mode (b), first and second modes (c), and third to fifth modes (d) in years after La Niña Modoki events.

All anomalies are averaged in the upper 30 m.

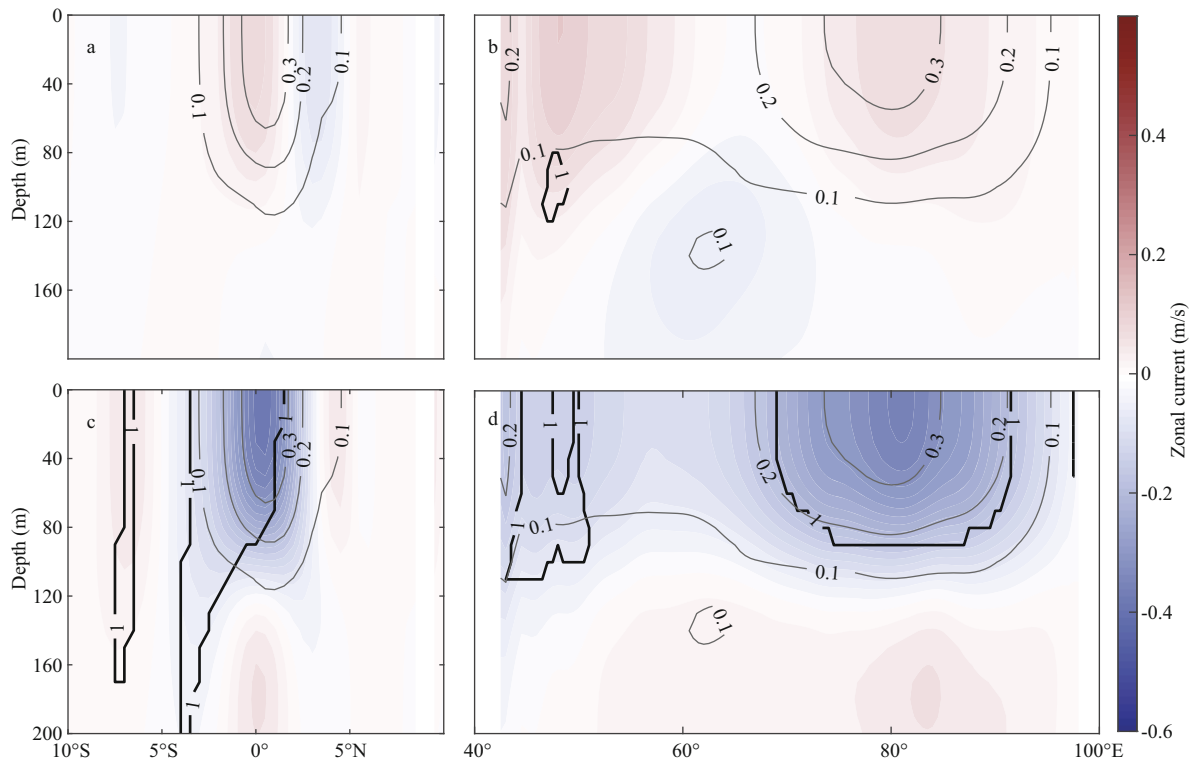


Fig.13 Same as Fig.8 except from the LCS model forced by ECMWF wind stress

The gray lines indicate the STD of zonal current and the values surrounded by the black contours are statistically significant at the 95% level.

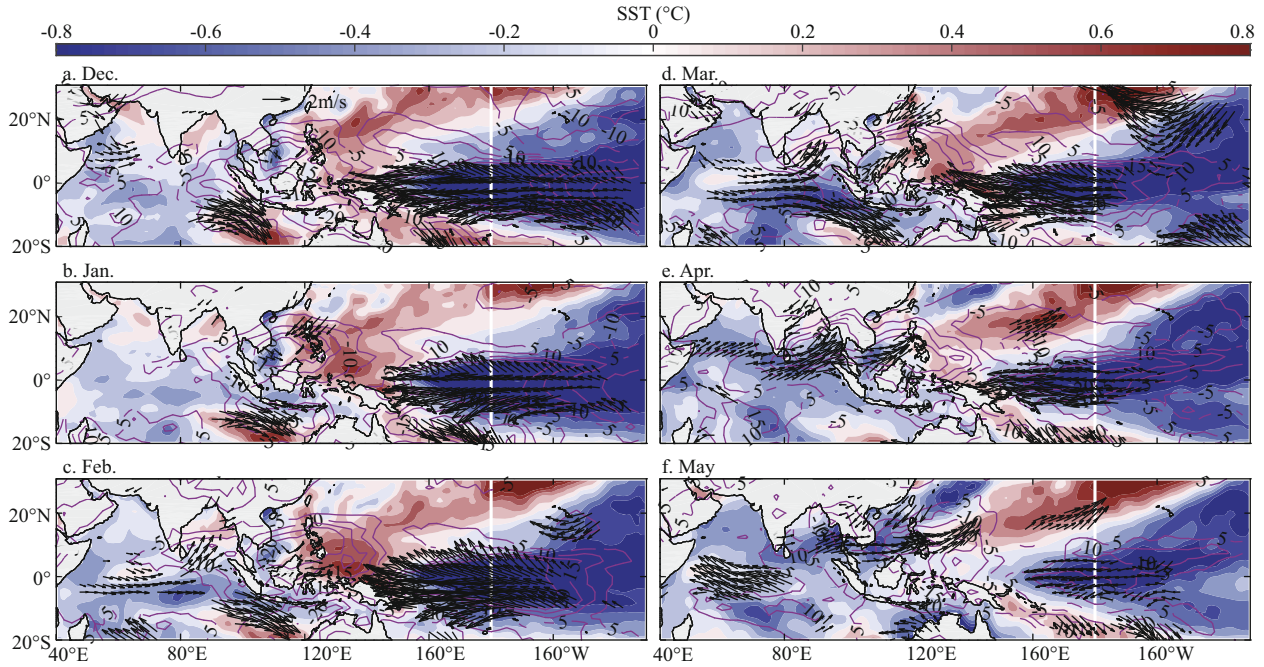


Fig.14 Sea surface temperature anomalies (shading, °C), OLR anomalies (contour, W/m^2) and wind anomalies (vector, m/s) after La Niña Modoki events

The wind statistically significant at the 90% level is shown.

eastern EIO since March which then gradually expand to the north and south and dominate the entire eastern and southeastern Indian Oceans (Fig.14e & f). In Fig.14, the OLR anomalies (contours) responded to

the SST anomalies shows that the center of enhanced convection located over the Indo-Pacific warm pool decays and moves eastward since March after the La Niña Modoki events. In April, the enhanced

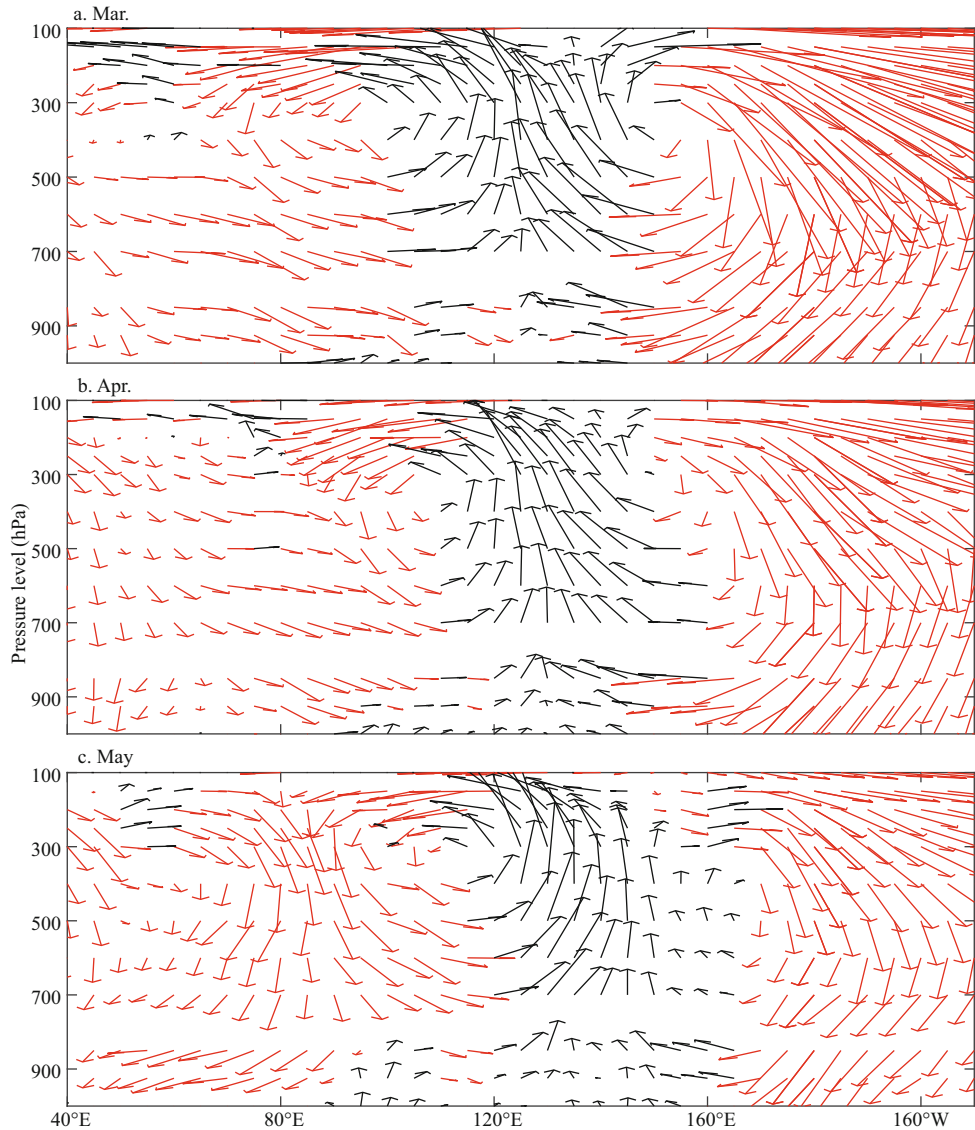


Fig.15 Composite map of the zonal-vertical wind (m/s, averaged between 5°S and 5°N) in March (a), April (b), May (c) after La Niña Modoki events

The vertical velocity has been multiplied by 1 000. The red vectors represent downward motion and the black upward.

convection in eastern Indian Ocean decays with the negative SST anomaly in the Maritime Continent and replace by the inhibited convection, and then it controls the entire eastern and southeastern Indian Ocean in May.

Regarding vertical distribution of the wind in May along the equator after the La Niña Modoki events (Fig.15), different position of the air downward motion leads to different wind anomalies in the low-level region. Before April, the air abnormally sinks west of 50°E and a westerly anomaly appears in the EIO. Then, the descending area appears over the center EIO in April, which induces a weak easterly anomaly in the western EIO. Until May, the center of downward motion locates in the region near 90°E .

This downward motion induces a strong surface easterly anomaly west of 90°E , sharply weakening the Wyrtki Jet. The weak positive SST anomaly mainly existed in southwestern Indian Ocean after El Niño Modoki events mainly affect the south part of Indian Ocean. Consequently, the weak Walker circulation in the equatorial region (no shown in this paper) makes less impact on the zonal wind anomaly in the EIO.

6 POTENTIAL REGIONAL IMPACT

Before the onset of the Indian summer monsoon, the spring Wyrtki Jet, which carry salty water from the western Indian Ocean to the eastern Indian Ocean, modulate the salinity in the upper ocean over the EIO.

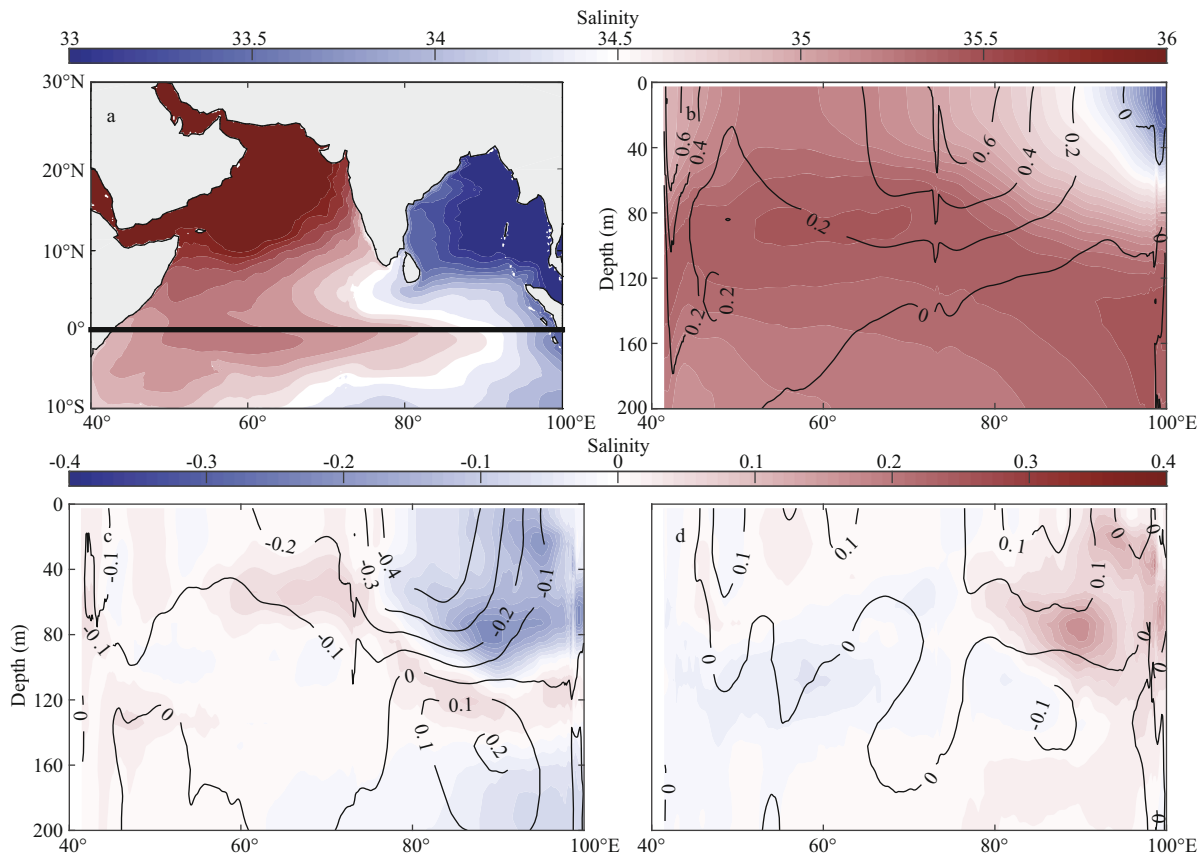


Fig.16 Map of climatology salinity in May averaged in the upper 30 m (a); longitude-depth diagram of climatology salinity in May (shading) and zonal current (contour, m/s) at 0°N section (averaged between 1°S and 1°N) (b); longitude-depth diagram of composite salinity anomalies (shading) in May in years after La Niña Modoki events (c) and El Niño Modoki events (d) at 0° section (average between 1°S and 1°N)

The contours indicate zonal current anomalies (m/s). All the datasets are from OFES. The darker straight line is the section of interest for this study.

The salinity variability affects the oceanic stratification. The impact of them on the TC intensification in the BoB has been reported (Ali et al., 2007; Sreenivas and Gnanaseelan, 2014). Based on the work we proposed in the previous section, we have discussed the horizontal and vertical structure of salinity anomalies in the Wyrtki Jet region after Niño Modoki events and its possible impact on the oceanic stratification.

Under the influence of the spring Wyrtki Jet, the most significant interannual anomaly of salinity exists in the eastern EIO (80°E–100°E, Fig.16). It corresponds to a significant zonal velocity anomaly (Fig.8c & d). After the El Niño Modoki events, the positive salinity anomaly appears mainly east of 80°E. A negative salinity anomaly is consistent with the zonal current anomaly in the upper 100 m in the eastern EIO after the La Niña Modoki events. Interestingly, after the El Niño Modoki events, the distribution of the salinity anomaly does not match that of the zonal current anomaly in the EIO. We

speculate that the weak zonal velocity anomaly has a little impact on the salinity anomaly and that the evaporation and precipitation may be the dominant factor for the salinity variability in the eastern Indian Ocean.

The salinity affects the buoyancy frequency that represents the oceanic stratification. We selected 2005 as a year after an El Niño Modoki event and 2008 as a year after a La Niña Modoki event for case study. In Fig.17, positive buoyancy frequency anomalous in May 2005 exist almost in the entire tropical Indian Ocean. In 2008, the positive (negative) buoyancy frequency anomaly exists in the western (eastern) tropical Indian Ocean. The negative buoyancy frequency anomaly is due to weaker subsurface salinity transport from west, as is indicated by the weaker spring Wyrtki Jet and zonal salinity gradient (Figs.8d & 16a). The sea surface temperature is modulated by the variability of oceanic stratification due to salinity in the upper ocean (Mooley and Parthasarathy, 1983). Higher sea surface temperature

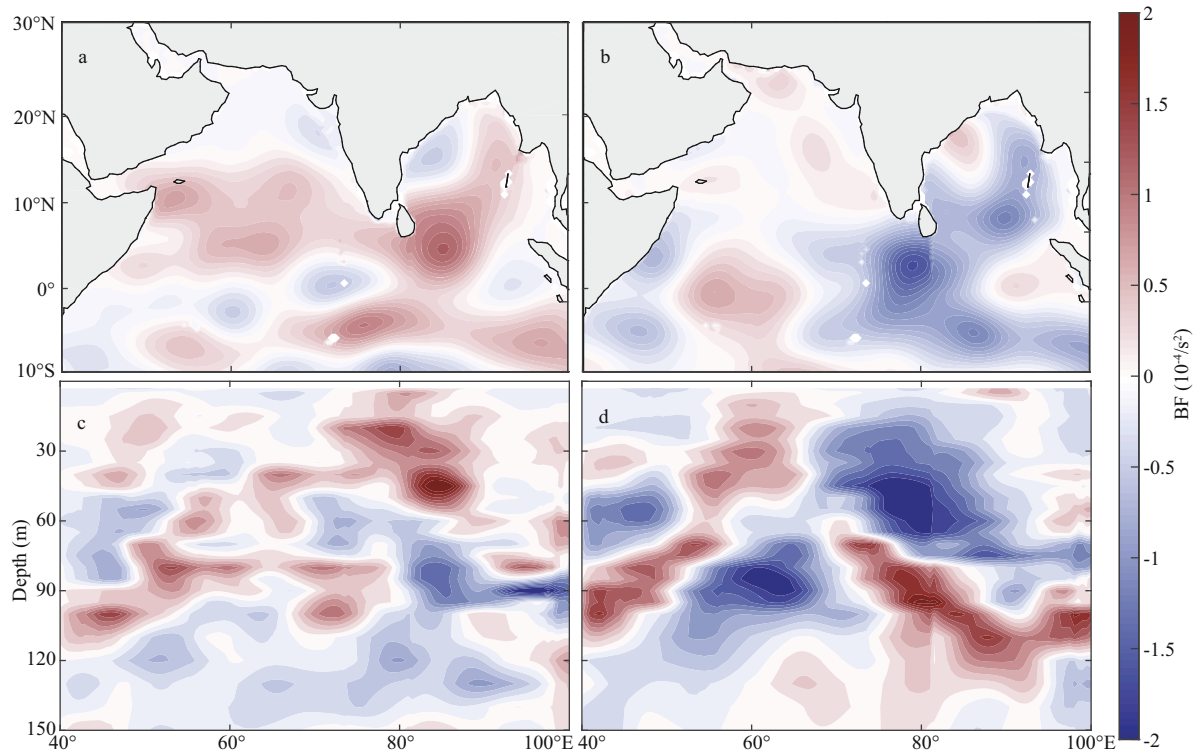


Fig.17 Map of buoyancy frequency (BF) anomalies ($10^{-4}/s^2$) in May 2005 (a), 2008 (b), averaged in the upper 30 m

c & d are at the same time as a & b except for the vertical distribution.

promotes the development of deep convection and enhances the rainfall in these regions (Chowdary et al., 2015, 2017). The spring Wyrtki Jet anomalies may have a possible impact on the variability of the local atmosphere and subsequent monsoon onset by altering the vertical salinity gradient anomalies in the EIO.

7 CONCLUSION

The investigation of the interannual variability of the spring Wyrtki Jet based on observations and model simulations indicates that there are remarkably anomalous behaviors of the jet and the relevant wind stress anomaly after Niño Modoki events. The westerly (strong easterly) wind anomaly leads to stronger (much weaker) spring Wyrtki Jets after El Niño (La Niña) Modoki events. The second baroclinic mode is the most important mode for the spring Wyrtki Jet anomaly. The first two baroclinic modes explain approximately 70% of the spring Wyrtki Jet anomaly, and the third to fifth modes together account for approximately 30%. The Niño Modoki events exert asymmetrical impact on the spring Wyrtki Jet. The El Niño Modoki events have no significant impact on the spring Wyrtki Jet, while the La Niña Modoki events reduce the strength of spring Wyrtki Jet. In addition, much weaker spring Wyrtki Jet can

influence the salinity and buoyancy frequency in the eastern Indian Ocean.

A schematic diagram explains the mechanism of the weakening of the spring Wyrtki Jet after the La Niña Modoki events (Fig.18). With strong negative SST and OLR anomalies on the surface eastern tropical Indian Ocean, the upper atmosphere sink in the eastern Indian Ocean and diverge in the lower troposphere. A strong easterly anomaly at the surface along the equator appears and induces much weaker spring Wyrtki Jet in the EIO.

8 ACKNOWLEDGMENT

The Ocean Surface Currents Analyses Real-time (OSCAR) surface current, Oceanic General Circulation Model for the Earth Simulator (OFES) current and salinity data and National Centers for Environmental Prediction (NCEP) wind field data were provided by the Asia-Pacific Data-Research Center of the IPRC (APDRC) <http://apdrc.soest.hawaii.edu/>. The Research Moored Array for African-Asian-Australian Monsoon Analysis and Prediction (RAMA) current data and SST data provided by National Oceanic and Atmospheric Administration were from <https://www.nodc.noaa.gov/>. Wind field data from the European Centre for

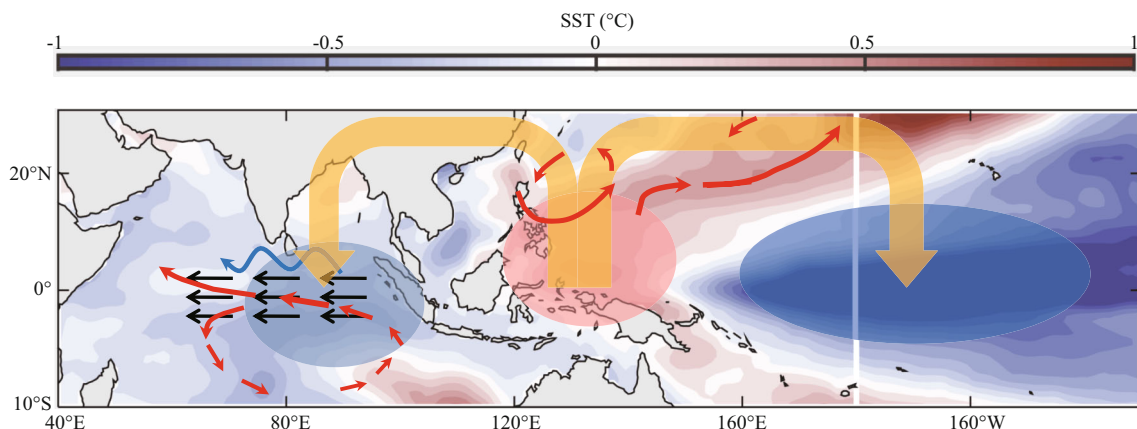


Fig.18 Schematic diagram for the change of atmospheric circulation and sea surface process during May after La Niña Modoki events

Oval red (blue) represents positive (negative) SST anomaly (basically consistent with OLR anomaly). Thickness or brightness of color represents the intensity. Red arrows represent low-level wind anomaly and yellow arrows represent Walker circulation. Blackarrows are the westward current anomaly and the blue curve arrow is the Rossby wave.

Medium-Range Weather Forecasts (ECMWF) product were obtained from <https://apps.ecmwf.int/datasets/>.

9 DATA AVAILABILITY STATEMENT

The OSCAR/OFES/NCEP datasets analyzed during the study are available in the [Asia-Pacific Data-Research Center of the IPRC (APDRC)] repository, (<http://apdrc.soest.hawaii.edu/>). The RAMA/OISST datasets analyzed during the study are available in the [National Oceanic and Atmospheric Administration (NOAA)] repository, (<https://www.nodc.noaa.gov/>). The ERA-I datasets analyzed during the study are available in the (European Centre for Medium-Range Weather Forecasts (ECMWF)) repository, (<https://apps.ecmwf.int/datasets/>).

The LCS model data generated during the study are available from the corresponding author on reasonable request.

References

- Alexander M A, Bladé I, Newman M, Lanzante J R, Lau N C, Scott J D. 2002. The atmospheric bridge: the influence of ENSO teleconnections on air-sea interaction over the global oceans. *Journal of Climate*, **15**(16): 2 205-2 231.
- Ali M M, Jagadeesh P V, Jain S. 2007. Effects of eddies on Bay of Bengal cyclone intensity. *Eos*, **88**(8): 93-95.
- Ashok K, Behera S K, Rao S A, Weng H Y, Yamagata T. 2007. El Niño Modoki and its possible teleconnection. *Journal of Geophysical Research: Oceans*, **112**(C11): C11007.
- Ashok K, Yamagata T. 2009. Climate change: the El Niño with a difference. *Nature*, **461**(7263): 481-484.
- Chatterjee A, Shankar D, McCreary Jr J P, Vinayachandran P N. 2013. Yanai waves in the western equatorial Indian Ocean. *Journal of Geophysical Research: Oceans*, **118**(3): 1 556-1 570.
- Chen G X, Han W Q, Li Y L, Wang D X, McPhaden M J. 2015. Seasonal-to-Interannual time-scale dynamics of the Equatorial Undercurrent in the Indian Ocean. *Journal of Physical Oceanography*, **45**(6): 1 532-1 553.
- Chen G X, Han W Q, Li Y L, Yao J L, Wang D X. 2019. Intraseasonal variability of the equatorial undercurrent in the Indian Ocean. *Journal of Physical Oceanography*, **49**(1): 85-101.
- Cheng X H, McCreary J P, Qiu B, Qi Y Q, Du Y. 2017. Intraseasonal-to-semiannual variability of sea-surface height in the astern, equatorial Indian Ocean and southern Bay of Bengal. *Journal of Geophysical Research: Oceans*, **122**(5): 4 051-4 067.
- Chowdary J S, Bandgar A B, Gnanaseelan C, Luo J J. 2015. Role of tropical Indian Ocean air-sea interactions in modulating Indian summer monsoon in a coupled model. *Atmospheric Science Letters*, **16**(2): 170-176.
- Chowdary J S, Harsha H S, Gnanaseelan C, Srinivas G, Parekh A, Pillai P, Naidu C V. 2017. Indian summer monsoon rainfall variability in response to differences in the decay phase of El Niño. *Climate Dynamics*, **48**(7-8): 2 707-2 727.
- Dandi R A, Chowdary J S, Pillai P A, Sidhan N S S, Koteswararao K, Ramakrishna S S S V S. 2020. Impact of El Niño Modoki on Indian summer monsoon rainfall: role of western north Pacific circulation in observations and CMIP5 models. *International Journal of Climatology*, **40**(4): 2 117-2 133.
- Dee D P, Uppala S M, Simmons A J, Berrisford P, Poli P, Kobayashi S, Andrae U, Balmaseda M A, Balsamo G, Bauer P, Bechtold P, Beljaars A C M, van de Berg L, Bidlot J, Bormann N, Delsol C, Dragani R, Fuentes M, Geer A J, Haimberger L, Healy S B, Hersbach H, Holm E V, Isaksen L, Källberg P, Köhler M, Matricardi M, McNally A P, Monge-Sanz B M, Morcrette J J, Park B K, Peubey C, de Rosnay P, Tavolato C, Thépaut J N, Vitart F.

2011. The ERA-Interim reanalysis: configuration and performance of the data assimilation system. *Quarterly Journal of the Royal Meteorological Society*, **137**(656): 553-597.
- Deshpande A, Gnanaseelan C, Chowdary J S, Rahul S. 2017. Interannual spring Wyrtki jet variability and its regional impacts. *Dynamics of Atmospheres and Oceans*, **78**: 26-37.
- Deshpande A, Gnanaseelan C. 2013. Interannual variability in Wyrtki jets and its impact on Indian Summer Monsoon circulation. In: AGU Fall Meeting Abstracts. AGU, Washington.
- Donguy J R, Meyers G. 1995. Observations of geostrophic transport variability in the western tropical Indian Ocean. *Deep Sea Research Part I: Oceanographic Research Papers*, **42**(6): 1 007-1 028.
- Duan Y L, Liu L, Han G Q, Liu H W, Yu W D, Yang G, Wang H W, Wang H Y, Liu Y L, Zahid, Waheed H. 2016. Anomalous behaviors of Wyrtki Jets in the equatorial Indian Ocean during 2013. *Scientific Reports*, **6**: 29688.
- Gnanaseelan C, Deshpande A, McPhaden M J. 2012. Impact of Indian Ocean Dipole and El Niño/southern oscillation wind-forcing on the Wyrtki jets. *Journal of Geophysical Research: Oceans*, **117**(C8): C08005.
- Han W Q, Lawrence D M, Webster P J. 2001. Dynamical response of equatorial Indian Ocean to intraseasonal winds: zonal flow. *Geophysical Research Letters*, **28**(22): 4 215-4 218.
- Han W Q, McCreary J P, Masumoto Y, Vialard J, Duncan B. 2011. Basin resonances in the equatorial Indian Ocean. *Journal of Physical Oceanography*, **41**(6): 1 252-1 270.
- Han W Q, McCreary Jr J P, Anderson D L T, Mariano A J. 1999. Dynamics of the eastern surface jets in the equatorial Indian Ocean. *Journal of Physical Oceanography*, **29**(9): 2 191-2 209.
- Han W Q. 2005. Origins and dynamics of the 90-day and 30-60-day variations in the equatorial Indian Ocean. *Journal of Physical Oceanography*, **35**(5): 708-728.
- Joseph S, Wallcraft A J, Jensen T G, Ravichandran M, Shenoi S S C, Nayak S. 2012. Weakening of spring Wyrtki jets in the Indian Ocean during 2006-2011. *Journal of Geophysical Research: Oceans*, **117**(C4): C04012.
- Klein S A, Soden B J, Lau N C. 1999. Remote sea surface temperature variations during ENSO: evidence for a tropical atmospheric bridge. *Journal of Climate*, **12**(4): 917-932.
- Knox R A. 1976. On a long series of measurements of Indian Ocean equatorial currents near Addu Atoll. *Deep Sea Research and Oceanographic Abstracts*, **23**(3): 211-221, IN1.
- Larkin N K, Harrison D E. 2005. Global seasonal temperature and precipitation anomalies during El Niño autumn and winter. *Geophysical Research Letters*, **32**(16): L16705.
- Lau K M, Wu H T. 2010. Characteristics of precipitation, cloud, and latent heating associated with the Madden-Julian oscillation. *Journal of Climate*, **23**(3): 504-518.
- Lau N C. 1997. Interactions between global SST anomalies and the midlatitude atmospheric circulation. *Bulletin of the American Meteorological Society*, **78**(1): 21-34.
- Lau W K M, Waliser D E. 2012. Intraseasonal Variability in the Atmosphere-Ocean Climate System. Springer, Berlin, Heidelberg.
- Masumoto Y, Hase H, Kuroda Y, Matsuura H, Takeuchi K. 2005. Intraseasonal variability in the upper layer currents observed in the eastern equatorial Indian Ocean. *Geophysical Research Letters*, **32**(2): L02607.
- Masumoto Y, Morioka Y, Sasaki H. 2008. High-resolution Indian Ocean simulations-Recent advances and issues from OFES. In: Hecht M W, Hasumi H eds. *Ocean Modeling in an Eddying Regime*. AGU, Washington. p.199-212.
- McCreary J P, Han W, Shankar D, Shetye S R. 1996. Dynamics of the east India coastal current: 2. Numerical solutions. *Journal of Geophysical Research: Oceans*, **101**(C6): 13 993-14 010.
- McPhaden M J, Wang Y, Ravichandran M. 2015. Volume transports of the Wyrtki jets and their relationship to the Indian Ocean Dipole. *Journal of Geophysical Research: Oceans*, **120**(8): 5 302-5 317.
- Miyama T, McCreary Jr J P, Jensen T G, Loschnigg J, Godfrey S, Ishida A. 2003. Structure and dynamics of the Indian-Ocean cross-equatorial cell. *Deep Sea Research Part II: Topical Studies in Oceanography*, **50**(12-13): 2 023-2 047.
- Miyama T, McCreary Jr J P, Sengupta D, Senan R. 2006. Dynamics of biweekly oscillations in the equatorial Indian Ocean. *Journal of Physical Oceanography*, **36**(5): 827-846.
- Molinari R L, Olson D, Reverdin G. 1990. Surface current distributions in the tropical Indian Ocean derived from compilations of surface buoy trajectories. *Journal of Geophysical Research: Oceans*, **95**(C5): 7 217-7 238.
- Mooley D A, Parthasarathy B. 1983. Variability of the Indian summer monsoon and tropical circulation features. *Mon. Wea. Rev.*, **111**(5): 967-978.
- Moum J N, de Szoeke S P, Smyth W D, Edson J B, DeWitt H L, Moulin A J, Thompson E J, Zappa C J, Rutledge S A, Johnson R H, Fairall C W. 2014. Air-sea interactions from westerly wind bursts during the November 2011 MJO in the Indian Ocean. *Bulletin of the American Meteorological Society*, **95**(8): 1 185-1 199.
- Nagura M, McPhaden M J. 2008. The dynamics of zonal current variations in the central equatorial Indian Ocean. *Geophysical Research Letters*, **35**(23): L23603.
- Nagura M, McPhaden M J. 2010a. Dynamics of zonal current variations associated with the Indian Ocean dipole. *Journal of Geophysical Research: Oceans*, **115**(C11): C11026.
- Nagura M, McPhaden M J. 2010b. Wyrtki jet dynamics: seasonal variability. *Journal of Geophysical Research: Oceans*, **115**(C7): C07009.
- Nyadjro E S, McPhaden M J. 2014. Variability of zonal currents in the eastern equatorial Indian Ocean on seasonal to interannual time scales. *Journal of Geophysical Research: Oceans*, **119**(11): 7 969-7 986.
- O'Brien J J, Hurlbert H E. 1974. Equatorial jet in the Indian

- Ocean: theory. *Science*, **184**(4141): 1 075-1 077.
- Prerna S, Chatterjee A, Mukherjee A, Ravichandran M, Shenoi S S C. 2019. Wyrtki Jets: role of intraseasonal forcing. *Journal of Earth System Science*, **128**(1): 21.
- Qiu Y, Li L, Yu W D. 2009. Behavior of the Wyrtki Jet observed with surface drifting buoys and satellite altimeter. *Geophysical Research Letters*, **36**(18): L18607.
- Rao S A, Gopalakrishna V V, Shetye S R, Yamagata T. 2002. Why were cool SST anomalies absent in the Bay of Bengal during the 1997 Indian Ocean Dipole Event? *Geophysical Research Letters*, **29**(11): 50-1-50-4.
- Reppin J, Schott F A, Fischer J, Quadfasel D. 1999. Equatorial currents and transports in the upper central Indian Ocean: annual cycle and interannual variability. *Journal of Geophysical Research: Oceans*, **104**(C7): 15 495-15 514.
- Sasaki H, Sasai Y, Kawahara S, Furuichi M, Araki F, Ishida A, Yamanaka Y, Masumoto Y, Sakuma H. 2004. A series of eddy-resolving ocean simulations in the world ocean-OFES (OGCM for the Earth Simulator) project. In: Oceans' 04 MTS/IEEE Techno-Ocean'04. IEEE, Kobe. p.1 535-1 541.
- Senan R, Sengupta D, Goswami B N. 2003. Intraseasonal "monsoon jets" in the equatorial Indian Ocean. *Geophysical Research Letters*, **30**(14): 1 750.
- Shinoda T, Hurlbert H E, Metzger E J. 2011. Anomalous tropical ocean circulation associated with La Niña Modoki. *Journal of Geophysical Research: Oceans*, **116**(C12): C12001.
- Sreenivas P, Chowdary J S, Gnanaseelan C. 2012. Impact of tropical cyclones on the intensity and phase propagation of fall Wyrtki jets. *Geophysical Research Letters*, **39**(22): L22603.
- Sreenivas P, Gnanaseelan C. 2014. Impact of oceanic processes on the life cycle of severe cyclonic storm "Jal". *IEEE Geoscience and Remote Sensing Letters*, **11**(2): 519-523.
- Srinivas G, Chowdary J S, Gnanaseelan C, Parekh A, Dandi R, Prasad K V S R, Naidu C V. 2019. Impact of differences in the decaying phase of El Niño on South and East Asia summer monsoon in CMIP5 models. *International Journal of Climatology*, **39**(14): 5 503-5 521.
- Subrahmanyam B, Murty V S N, Heffner D M. 2011. Sea surface salinity variability in the tropical Indian Ocean. *Remote Sensing of Environment*, **115**(3): 944-956.
- Suresh I, Vialard J, Lengaigne M, Han W, McCreary J, Durand F, Muraleedharan P M. 2013. Origins of wind-driven intraseasonal sea level variations in the North Indian Ocean coastal waveguide. *Geophysical Research Letters*, **40**(21): 5 740-5 744.
- Thompson B, Gnanaseelan C, Salvekar P S. 2006. Variability in the Indian Ocean circulation and salinity and its impact on SST anomalies during dipole events. *Journal of Marine Research*, **64**(6): 853-880.
- Wang J. 2017. Observational bifurcation of Wyrtki Jets and its influence on the salinity balance in the eastern Indian Ocean. *Atmospheric and Oceanic Science Letters*, **10**(1): 36-43.
- Wang X, Tan W, Wang C Z. 2018. A new index for identifying different types of El Niño Modoki events. *Climate Dynamics*, **50**(7-8): 2 753-2 765.
- Wyrtki K. 1973. An equatorial jet in the Indian Ocean. *Science*, **181**(4096): 262-264.
- Xie S P, Annamalai H, Schott F A, McCreary Jr J P. 2002. Structure and mechanisms of South Indian Ocean climate variability. *Journal of Climate*, **15**(8): 864-878.
- Xie S P, Deser C, Vecchi G A, Ma J, Teng H Y, Wittenberg A T. 2010. Global warming pattern formation: sea surface temperature and rainfall. *Journal of Climate*, **23**(4): 966-986.
- Xie S P, Hu K M, Hafner J, Tokinaga H, Du Y, Huang G, Sampe T. 2009. Indian Ocean capacitor effect on Indo-western Pacific climate during the summer following El Niño. *Journal of Climate*, **22**(3): 730-747.
- Xie S P, Kosaka Y, Du Y, Hu K M, Chowdary J S, Huang G. 2016. Indo-western Pacific ocean capacitor and coherent climate anomalies in post-ENSO summer: a review. *Advances in Atmospheric Sciences*, **33**(4): 411-432.
- Yeh S W, Kug J S, Dewitte B, Kwon M H, Kirtman B P, Jin F F. 2009. El Niño in a changing climate. *Nature*, **461**(7263): 511-514.
- Yu J Y, Kao H Y. 2007. Decadal changes of ENSO persistence barrier in SST and ocean heat content indices: 1958-2001. *Journal of Geophysical Research: Atmospheres*, **112**(D13): D13106.
- Yuan Y, Yan H M. 2013. Different types of La Niña events and different responses of the tropical atmosphere. *Chinese Science Bulletin*, **58**(3): 406-415.
- Zhang D X, McPhaden M J, Lee T. 2014. Observed interannual variability of zonal currents in the equatorial Indian Ocean thermocline and their relation to Indian Ocean Dipole. *Geophysical Research Letters*, **41**(22): 7 933-7 941.
- Zhang Y, Du Y, Zhang Y H, Gao S. 2016. Asymmetry of upper ocean salinity response to the Indian Ocean dipole events as seen from ECCO simulation. *Acta Oceanologica Sinica*, **35**(7): 42-49.